JOC The Journal of Organic Chemistry

Article

pubs.acs.org/joc

Synthesis and Linear and Nonlinear Optical Properties of Three Push−Pull Oxazol-5(4*H*)-one Compounds

Beata Jędrzejewska,*[,†] Marta Gordel,[‡,§] Janusz Szeremeta,[‡] Przemysław Krawczyk,[∥] and Marek Samoć[‡]

[†]University of Technology and Life Sciences, Faculty of Chemical Technology and Engineering, Seminaryjna 3, 85-326 Bydgoszcz, Poland

[‡]Wroclaw University of Technology, Faculty of Chemistry, Advanced Materials Engineering and Modelling Group, Wybrzeże Wyspiańskiego 27, 50-370 Wroclaw, Poland

[§]Laboratory of Biology and Applied Pharmacology, CNRS, Ecole Normale Superieure de Cachan, 61 Avenue du President Wilson, 94235 Cachan, France

[∥]Nicolaus Copernicus University, Collegium Medicum, Department of Physical Chemistry, Kurpińskiego 5, 85-950 Bydgoszcz, Poland

Supporting Information

ABSTRACT: Three uncharged push−pull oxazol-5(4*H*)-ones were synthesized and thoroughly characterized. The examined molecules contained electron-donor and electron-acceptor groups interacting via a π-conjugated bridge. Spectral properties of the oxazol-5(4*H*)-ones were studied in detail in three solvents of different polarities. The results indicate a solvatochromic shift toward lower energy for the charge-transfer state. The compounds are weakly fluorescent in polar solvents, but they have high fluorescence quantum yields in nonpolar solvents. Their two-photon absorption (2PA) properties were characterized by the open- and closed-aperture Z-scan technique, by the pump−probe technique, and by the two-photon excited fluorescence method. The dyes exhibit relatively high effective two-photon absorption cross sections ranging from 490 to 2600 GM at ~100 GW/cm^2, according to the Z-scan results, which are found, however, to contain significant contribution from higher-order absorption processes. In addition, these compounds display good photostability.

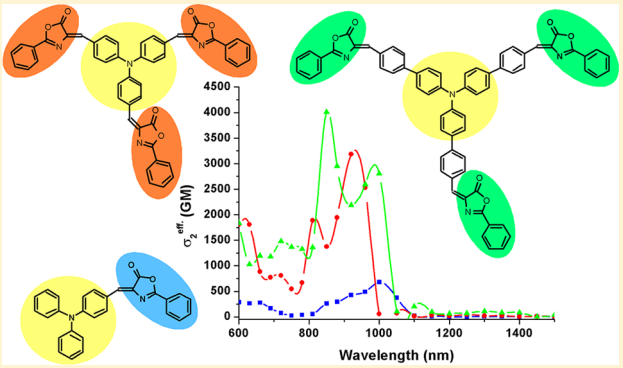

INTRODUCTION

Organic compounds which exhibit a large nonlinear optical (NLO) response, in particular those showing sizable nonlinear absorption effects such as two-photon absorption (2PA), have a number of applications such as three-dimensional (3D) optical data storage, 3D optical imaging for biological systems, 3D microfabrication and early corrosion detection, optical power limiting and photodynamic therapy, etc.[1,2] The need for finding materials optimized for these applications has spurred the interest in development of new molecules and structures with enhanced 2PA properties. The nonlinear process of two-photon absorption involves electronic excitation of a molecule through a simultaneous action of a pair of photons of the same or different energies.[3] It can be quantified experimentally by assessing the value of the 2PA cross-section, σ_2.[3,4] This parameter can be determined from two-photon excited fluorescence[5] or thermo-optical methods[6] or directly by transmittance measurements in the Z-scan technique.[7]

The fluorescence method[5,8] is based on measurements of the fluorescence signal from the 2PA excited state. It requires a carefully chosen reference sample and validation of the quadratic dependence of the intensity of two-photon excited fluorescence (2PEF) on the intensity of exciting radiation.[9]

The thermo-optical methods include photoacoustic and thermal-lens techniques,[10] both being based on the detection of the temperature rise following the conversion of absorbed optical radiation into heat through nonradiative relaxation processes. The former technique is based on the generation of acoustic waves in the sample,[11] whereas thermal lens spectroscopy detects a change in the refractive index of the solvent.[12]

The Z-scan technique is a method which can simultaneously measure both nonlinear absorption (NLA) coefficient and nonlinear refractive index (NLR) in samples that typically are solid plates, films, or liquid solutions.[13,14] In the Z-scan experiment, a laser beam is focused to a minimum waist at the focal point which corresponds to the value of $z = 0$, where z is the propagation direction (z axis) of the beam.[7,15] A sample is then made to traverse the path along that of the beam, with

Received: July 15, 2015
Published: August 28, 2015

DOI: 10.1021/acs.joc.5b01636
J. Org. Chem. 2015, 80, 9641−9651

variations of the incident intensity resulting in distortion and changes in transmittance of the beam which are probed by two detectors: so-called open-aperture and closed-aperture detectors. Analysis of the results obtained for a sample, which may be a solution of an investigated chromophore in a cell, leads to determination of microscopic parameters such as the complex hyperpolarizability γ and the two-photon cross section σ_2.

The 2PA cross section can be also estimated theoretically on the basis of different types of computational methods such as ab initio and semiempirical.[16] Semiempirical models have somewhat limited quantitative performance, because the nonlinear spectra are typically dominated by higher excitation levels involving significant electronic correlations. In turn, ab initio methods exist as two large families of methods: Hartree−Fock and density functional.[16] Adiabatic time-dependent density functional theory (TD-DFT) for the calculations of molecular nonlinear optical properties has been suggested on the basis of the residues of the quadratic response functions for 2PA[17] and on the quasi-particle formalism of the time-dependent Kohn−Sham (TD-KS) equations for the arbitrary frequency-dependent nonlinear optical polarizabilities.[18] The overall performance of TD-DFT methods is found to be good in combination with proper functionals and basis sets.[16]

Organic molecules with large 2PA cross sections may differ in their structures.[19] They may be linear[20] or branched[21−23] π-conjugated organic compounds with a symmetrical or asymmetrical arrangement of electron-donor (D) and electron-acceptor (A) groups. The influences of different molecular conjugation lengths, types of conjugated cores and the periphery sites, molecular dimensionalities, and the planarities of the central parts of organic molecules on their TPA properties have been explored in great detail.[24]

The present study was undertaken in order to reveal the linear and nonlinear optical properties of three oxazolone derivatives; the experimental results are supplemented with theoretical simulations. The description of syntheses of the three compounds **4**−**6** and their full spectroscopic characterization are also included.

RESULTS AND DISCUSSION

Synthesis. The synthesis of the oxazolone derivatives **4**−**6** is shown in Scheme 2. The starting aldehydes **1** and **2** are available commercially, while **3** was prepared from tris(4-bromophenyl)amine by Suzuki coupling with 4-formylbenzeneboronic acid according to a published procedure (Scheme 1).[25] The "Erlenmeyer azlactone synthesis"[26] was applied to obtain the oxazolone derivatives. The condensation of hippuric acid with the aldehydes in acetic anhydride[27] afforded compounds **4**−**6** in 57.6%, 52.8%, and 49.6% yields, respectively. It should be noted that the synthesis of compound **4** was reported recently by, for example, Ramanathan et al.[28] (4*Z*)-4-[4-(Diphenylamino)benzylidene]-2-phenyl-1,3-oxazol-5(4*H*)-one (**4**) was used as a benchmark molecule for the optical property studies. Compounds **5** and **6** have a C_3-symmetric structure with electron-withdrawing groups (2-phenyloxazolone) introduced onto the triphenylamine or tris[1-(4,4′-biphenyl)]amine core at the periphery sites, in contrast to compound **4**, which has an asymmetric structure. ^{1}H NMR, ^{13}C NMR spectroscopy, HPLC chromatography, and elemental analysis were used to identify the chemical structure and purity of all of these chromophores (see the Experimental Section and the Supporting Information).

One-Photon UV−Vis Spectral Properties. The electronic absorption and fluorescence spectra of the three oxazolone derivatives were recorded in three solvents of different polarities. The corresponding absorption λ_{abs} and emission λ_{fl} maxima, the fluorescence quantum yields Φ_{fl}, and the fluorescence lifetimes of the dyes under study are collected in Table 1. Figure 1 illustrates the absorption and emission properties of the tested compounds in THF. The electronic absorption spectra show two peaks in the 300−400 and 460−505 nm regions, corresponding to the $S_0 \rightarrow S_2$ and $S_0 \rightarrow S_1$ transitions, respectively. The lower energy strong absorption band can be attributed to the charge-transfer (CT) transition of the dye involving transfer between the electron-donating triphenylamine moiety and the electron-withdrawing oxazolone. The compound **5** with a symmetrically substituted triphenylamine core shows a red shift of its absorption band in comparison to the asymmetrical dye (**4**). However, a slight blue shift in the absorption maximum was observed when additional phenyl groups were incorporated in the symmetrical derivative. This effect can be assigned to the different charge distributions within the molecule. The molecule of **4** has a typical push−pull structure with an absorption maximum at ca. 470 nm. The red shift observed for the branched dye **5** in comparison to its monomeric equivalent can be assigned to the increase of electron affinity of the electron-accepting moiety of the light-absorbing chromophore. On the other hand, the hypsochromic effect observed for compound **6** may be attributed to an elongation of the π system which results in a decrease in the effectiveness of charge transfer between the electron donor (triphenylamine) and the electron acceptor (2-phenyloxazolone) moieties caused by the internal rotation.

Furthermore, the one-photon absorption (1PA) strength of the CT state is highly enhanced by branching: for instance, the 1PA intensity of the CT state for compounds **5** and **6** is ca. twice as large as that for compound **4**. However, when we compare the reduced molar absorbances, which can be defined as ε_{max} divided by the molecular weight (MW),[22] the enhancement is clear only for compound **5**. This can be assigned to the extended π delocalization and a certain coupling between the branches in dye **5**. In the case of dye **6** the reduced molar absorbance is lower than that for compound **4**: i.e., incorporating more phenyl rings into the central triphenylamine moiety does not increase ε_{max} by the same factor as the molecular weight.

Steady-state fluorescence spectra for the samples in THF show emission bands at ca. 572 and 582 nm for **4** and **5**, respectively; in the case of **6** the fluorescence band is red-shifted to 635 nm. The fluorescence spectra exhibit a single peak (cf. Figure 1), suggesting that the emission occurs from the lowest excited state only.

In order to characterize the optical properties of the oxazolone derivatives with finer detail, we analyzed their absorption and emission spectra in solvents of different polarities. The main absorption bands with maxima at 475, 506, and 459 nm in toluene shift to 471, 504, and 460 nm in DMF for **4**−**6**, respectively. Thus, the absorption does not exhibit any significant solvent shift. In contrast, the solvent polarity affects the fluorescence spectra to a great extent. All compounds reveal positive solvatochromic behavior. The largest solvent shift of the fluorescence band was observed for **6**. The fluorescence band shows a shift of about 2900 cm^{-1} for **4** and **5** and ca. 5210 cm^{-1} for **6** on changing the solvent from toluene to DMF. The large bathochromic shifts of the

DOI: 10.1021/acs.joc.5b01636
J. Org. Chem. 2015, 80, 9641−9651

Table 1. Photophysical Data[a] for Compounds 4–6

compd	solvent	λ_{max}^{ab} (ε_{max})	ε_{max}/MW	δ_1^{PA}	λ_{max}^{fl}	$\Delta\nu$	Φ_{fl}	τ_1^{fl} (α_1)	τ_2^{fl} (α_2)	τ_3^{fl} (α_3)	τ_{av}^{fl}	χ^2	k_r	k_{nr}	f_{os}
4	toluene	475.5 (5.41)	129.9	2.07	530.4	2177	0.034	0.025 (21.6)	0.283 (75.4)	1.989 (3.00)	0.278	1.171	1.21	34.7	0.73
	THF	469 (4.86)	116.7	1.86	571.6	3827	0.108	0.37 (8.2)	1.309 (91.8)		1.232	1.145	0.87	7.24	0.74
	DMF	471 (4.36)	104.7	1.67	627	5282	0.014	0.035 (4.9)	0.302 (93.9)	1.211 (1.2)	0.300	1.087	0.47	32.9	0.70
5	toluene	505.5 (10.85)	143.0	4.15	541.6	1319	0.395	0.284 (7.4)	2.096 (92.6)		1.961	1.413	2.01	3.09	1.29
	THF	500 (10.43)	137.4	3.98	582	2818	0.340	0.531 (7.2)	2.621 (92.8)		2.471	1.444	1.38	2.67	1.57
	DMF	504 (9.50)	125.2	3.63	640.6	4231	0.0042	0.199 (93.1)	1.45 (6.9)		0.286	1.186	0.15	34.8	1.62
6	toluene	459 (11.71)	118.6	4.47	535	3095	0.475	0.549 (12.7)	2.013 (87.3)		1.826	1.204	2.60	2.88	1.78
	THF	459 (10.76)	109.0	4.11	635	6038	0.297	0.538 (3.6)	2.783 (96.4)		2.702	1.44	1.10	2.60	1.89
	DMF	460 (8.92)	90.33	3.41	741.8	8258	0.0015	0.074 (99.2)	1.480 (0.8)		0.085	1.259	0.18	117.1	1.67

[a]Definitions and units: absorption maxiumum (λ_{max}^{ab}), nm; fluorescence maximum (λ_{max}^{fl}), nm; shift ($\Delta\nu$), cm^{-1}; maximum extinction coefficient (ε_{max}), 10^4 M^{-1} cm^{-1}; reduced molar absorbance (ε_{max}/MW), dm^3 cm^{-1} g^{-1}; one-photon absorption cross section (δ_1^{PA}), Å^2; fluorescence quantum yield (Φ_{fl}); fluorescence lifetime (τ), ns; component amplitudes (α), %; correlation coefficients (χ^2); radiative (k_r) and nonradiative (k_{nr}) rate constants, 10^8 s^{-1}; oscillator strength (f_{os}).

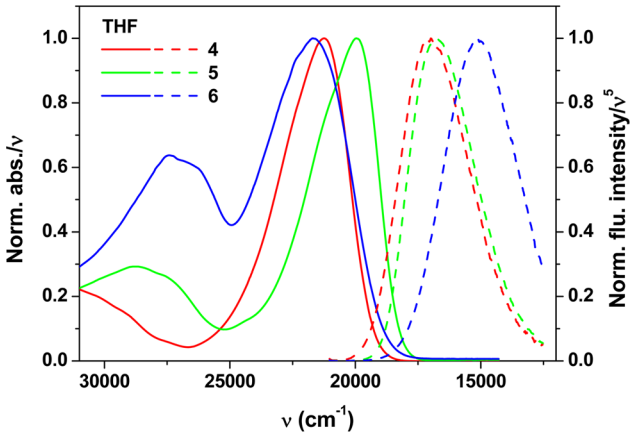

Figure 1. Normalized and scaled[29,30] electronic absorption (solid lines) and fluorescence (dashed lines) spectra of **4**–**6** in THF at room temperature; λ_{EX} 470 nm.

emission band with increasing solvent polarity indicate greater stabilization of the excited singlet state in polar solvents. Such behavior is characteristic for compounds showing more polar character in the excited state and having enlarged dipole moments and CT characters in that state.[31,32]

The observed large Stokes shifts (5282, 4231, and 8258 cm^{-1} for **4**–**6** in DMF, respectively) indicate that significant charge redistribution occurs upon excitation, prior to emission, and that the emission originates from a strongly dipolar emissive state.[33]

All chromophores under study display moderate emission in THF solution, with fluorescence quantum yields ranging from 0.108 (**4**) to 0.34 and 0.297 (**5** and **6**). The highest fluorescence quantum yields were determined, according to eq 1 (vide infra), in nonpolar solvent (Table 1) for the branched compounds (**5** and **6**). However, they are almost nonfluorescent in a polar solvent. Generally, an increase in the dimensionality of the molecule increases the quantum yield, and the yield reaches higher values when the polarity of the solvent decreases.

We also measured the fluorescence lifetimes of the dyes in solvents of different polarity. Figure 2 shows the emission decay of the studied dyes in THF after excitation at 466 nm. The emission is observed at 580 or 630 nm, corresponding to the

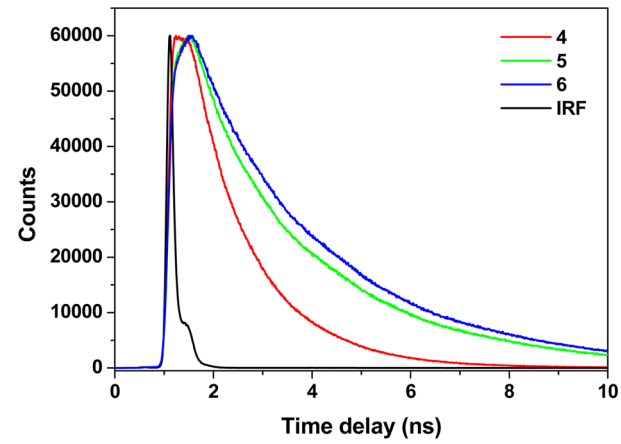

Figure 2. Fluorescence decay curves of compounds **4**–**6** recorded in THF: λ_{EX} 466 nm and λ_{EM} 580 and 630 nm for **4**–**6**, respectively. The black line is the instrument response function (IRF).

DOI: 10.1021/acs.joc.5b01636
J. Org. Chem. 2015, 80, 9641–9651

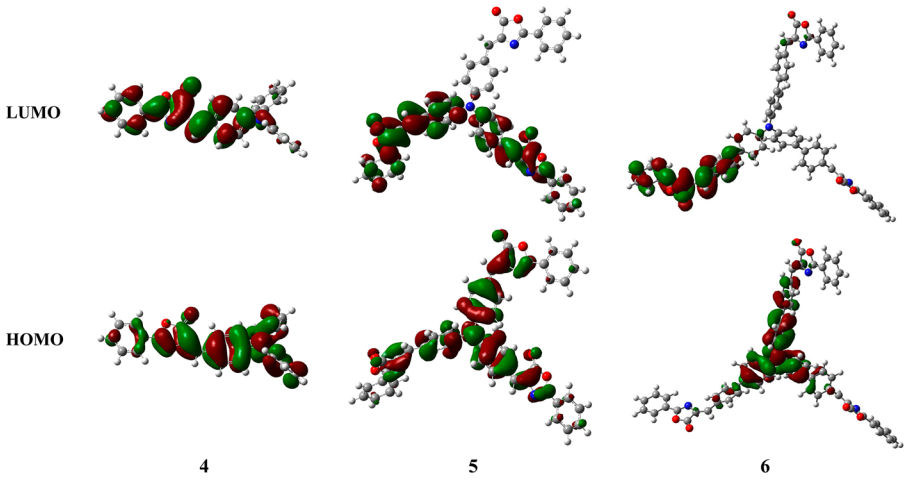

Figure 3. Frontier orbitals involved in the lowest-energy excitation for dyes **4**–**6** in the gas phase. The molecular orbitals were calculated at the CAM-B3LYP/6-311++G(d,p) level of theory under vacuum. Shown here are the contour surfaces of orbital amplitudes 0.02 (red) and −0.02 (green).

maximum of the fluorescence intensity. The decay time can be well fitted with a two-exponential function, giving fluorescence lifetimes of 538 and 2.783 ns.

Generally, the linear push−pull compound exhibits a three-exponential decay while the star-type three-branched dyes have two-exponential decays with a fast relaxation mechanism having a lifetime of a few hundred picoseconds followed by a slower mechanism on the nanosecond time scale. The fast fluorescence decay mechanism might be attributed to relaxation from the locally excited state toward an intramolecular charge transfer (ICT) state.[34,35] The formation of an ICT state is accompanied by a charge-transfer process from the electron-donating core to the electron-accepting edge substituents.[34] Additionally, the obtained results indicate that the calculated average fluorescence lifetimes do not correlate with the fluorescence quantum yields for different chromophores in the same solvent. The lack of correlation might be due to different radiative decay rates of these chromophores because of their different electronic structures.[33]

In order to see the CT process more clearly, molecular orbital surfaces of the HOMO and LUMO for the ground state of the studied dyes in the gas phase have been visualized in Figure 3. The shapes of the two frontier orbitals for compounds **4**–**6** confirm that the electrons move from the electron-donor to the electron-acceptor group. For instance, in the case of the dipolar molecule **4** the electrons are transferred from the diphenylamino to the 2-phenyloxazolone moiety, a typical feature of the CT state.[33−35] For **5**, the density polarization mainly occurs within one arm of the star-type three-branched compound. Electrons are moved from the 4-benzylidene-2-phenyl-1,3-oxazol-5(4*H*)-one moiety toward the remainder of the molecule. This effect is even more pronounced for dye **6**.

The calculated HOMO−LUMO energy gaps for **4**–**6** are 2.84, 2.54, and 3.40 eV, respectively. From these results it is apparent that electron transfer from the HOMO to the LUMO in **5** is relatively easier than that in **4**. Thus, in comparison to **4**, a bathochromic shift of **5** is observed in the electronic absorption spectrum. In contrast, the HOMO−LUMO energy gap of the dye **6** is higher than that of the linear compound **4** and a hypsochromic shift is observed. These results are consistent with those from the experiments.

The computations confirm that different density polarizations take place for the studied compounds, indeed resulting in an excited state that is more polar than the ground state and hence is better stabilized by polar solvents.[33−35]

Applications of fluorescent dyes in biolabeling and bioimaging require a good photostability of the candidate compounds. Photobleaching of the three chromophores **4**–**6** was studied in chloroform, ethyl acetate, acetonitrile, and THF. After more than 3 h of irradiation the absorption intensity in THF decreased by about 7%, 18%, and 3% for **4**–**6**, respectively.

Figure 4 shows the spectral changes that occur in the electronic absorption spectra of compound **6** on irradiation

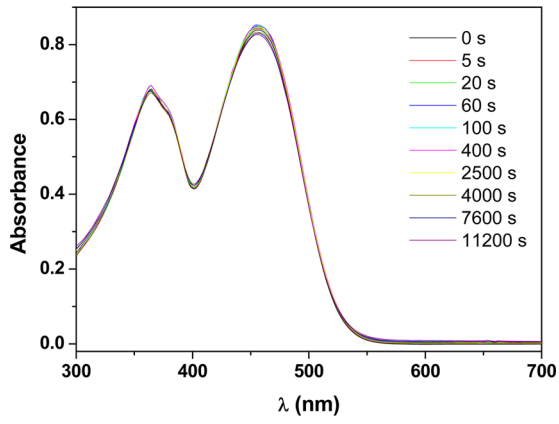

Figure 4. Changes in the electronic absorption spectra of dye **6** in THF after different times of irradiation with a laser (50 mW, 457 nm).

with a diode-pumped solid-state (DPSS) laser at 457 nm (50 mW). Upon irradiation no significant changes in the strength of the main absorption band and its location were observed. The more pronounced effect on the absorption intensity was only observed under irradiation for compound **5** in THF and acetonitrile. This confirms that the studied dyes are photochemically stable for short times of irradiation.

Two-Photon Spectral Properties. The structures of the compounds were designed to enable the newly synthesized push−pull oxazol-5(4*H*)-ones to possess potentially large two-

DOI: 10.1021/acs.joc.5b01636
J. Org. Chem. 2015, 80, 9641−9651

photon absorption (2PA) cross sections suitable for applications as 2PA fluorophores. To establish this, the nonlinear optical properties of the dyes were investigated. The parameters characterizing the nonlinear absorption and refraction of dyes **4**–**6** were determined by various techniques in order to confirm the obtained results.

Z-Scan Technique. To characterize the nonlinear absorption and refraction of the dyes, open- and closed-aperture Z-scan measurements were performed over a broad wavelength range (600–1600 nm). Spectra of nonlinear absorption for **4**–**6** are presented in Figures 5–7, respectively.

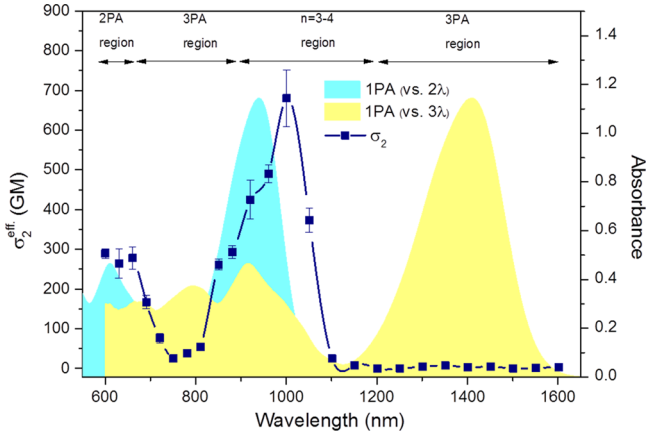

Figure 5. Diagram of nonlinear absorption strength at different wavelengths in the visible and infrared regions for **4**. $\sigma_2^{eff.}$ values for **4** are plotted as navy blue filled squares for a corresponding wavelength (the navy blue solid line is used to guide the eye). Cyan areas represent the 1PA spectra vs 2λ, and yellow areas represent the same 1PA spectra vs 3λ. 2PA was observed in the range between 600 and 660 nm and 3PA in the range between 690 and 820 nm and 1200–1600 nm. The Z-scan data indicate processes intermediate between 3PA and 4PA between 920 and 1150 nm.

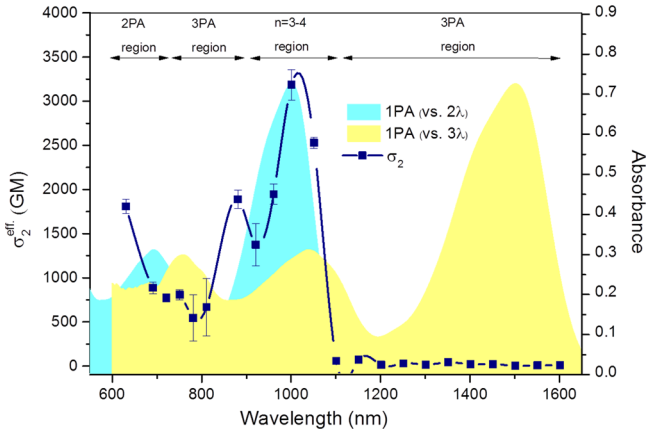

Figure 6. Diagram of nonlinear absorption strength at different wavelengths in the visible and infrared regions for **5**. $\sigma_2^{eff.}$ values for **5** are plotted as navy blue filled squares for a corresponding wavelength (the navy blue solid line is used to guide the eye). Cyan areas represent the 1PA spectra vs 2λ, and yellow areas represent the same 1PA spectra vs 3λ. 2PA was observed in the range between 600 and 690 nm and 3PA in the range between 720 and 850 nm and 1150–1600 nm. The Z-scan data indicate processes intermediate between 3PA and 4PA between 880 and 1100 nm.

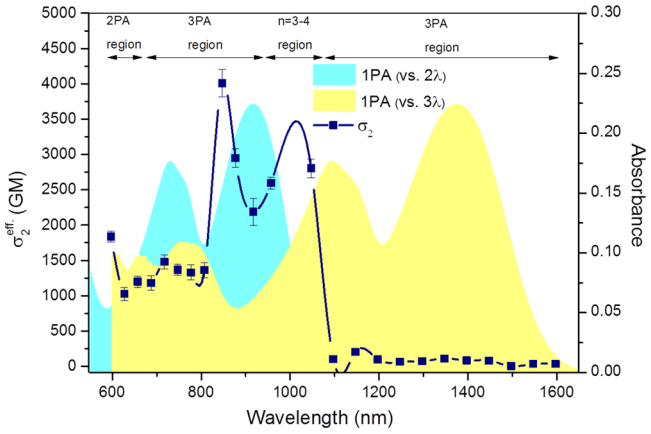

Figure 7. Diagram of nonlinear absorption strength at different wavelengths in the visible and infrared regions for **6**. $\sigma_2^{eff.}$ values for **6** are plotted as navy blue filled squares for a corresponding wavelength (the navy blue solid line is used to guide the eye). Cyan areas represent the 1PA spectra vs 2λ, and yellow areas represent the same 1PA spectra vs 3λ. 2PA was observed in the range between 600 and 660 nm and 3PA in the range between 690 and 920 nm and 1100–1600 nm. The Z-scan data indicate processes intermediate between 3PA and 4PA between 960 and 1050 nm.

Figure 5 shows nonlinear absorption spectra for **4** presented as effective two-photon absorption cross sections (σ_2^{eff}) vs wavelength of the incident photons. It needs to be explained that the Z-scan data have been processed here formally as due to a two-photon process; however, doubts arose whether actually the observed open-aperture Z-scan traces were caused by 2PA alone because the noticeable narrowing of the open aperture trace dips in comparison to theoretically predicted trace, which is a tell-tale sign of the existence of higher-order (multiphoton) processes. It is possible to exploit this narrowing to evaluate the effective number of photons which are in fact absorbed, giving rise to the observed transmittance changes.[36,37] Using this approach, we established that in fact only in the range between 600 and 660 nm is a clean 2PA process observed, followed by the dominance of 3PA in the ranges between 690 and 820 nm and 1200–1600 nm. To facilitate interpretation of the results, Figure 5 (and Figures 6 and 7) also include the shapes of the 1PA spectrum of the compound replotted against doubled and tripled wavelengths; thus, it is possible to see which states accessible through 1PA may also be reached by absorption of two or three photons. It is found that in the wavelength range of the overlap of 1PA spectra vs 2λ and 1PA spectra vs 3λ with the Z-scan data the number of absorbed photons is indeed not 2 but is between 3 and 4 (Figure 8d). The highest σ_2^{eff} value was recorded at 1000 nm, equal to 680 ± 70 GM. An identical measurement was carried out on **5** (Figure 6). Similar to the case for the dye **4**, at the shorter wavelength for **5** shows 2PA, which then gives way to 3PA at longer wavelengths. The highest σ_2^{eff} value was measured at 1000 nm, which is the maximum of 1PA vs 2λ and is 3200 ± 170 GM. The same procedure of determination of nonlinear optical properties by the Z-scan technique was followed for **6** (Figure 7). The dye seems to be a very efficient multiphoton absorber, the maximum σ_2^{eff} value being 4000 ± 200 GM (at 850 nm).

Representative closed-aperture (CA) and open-aperture (OA) Z-scan traces for dyes **4**–**6** at 111 GW cm^{-2} with femtosecond pulses at 960 nm are presented in Figure 8. The

DOI: 10.1021/acs.joc.5b01636
J. Org. Chem. 2015, 80, 9641–9651

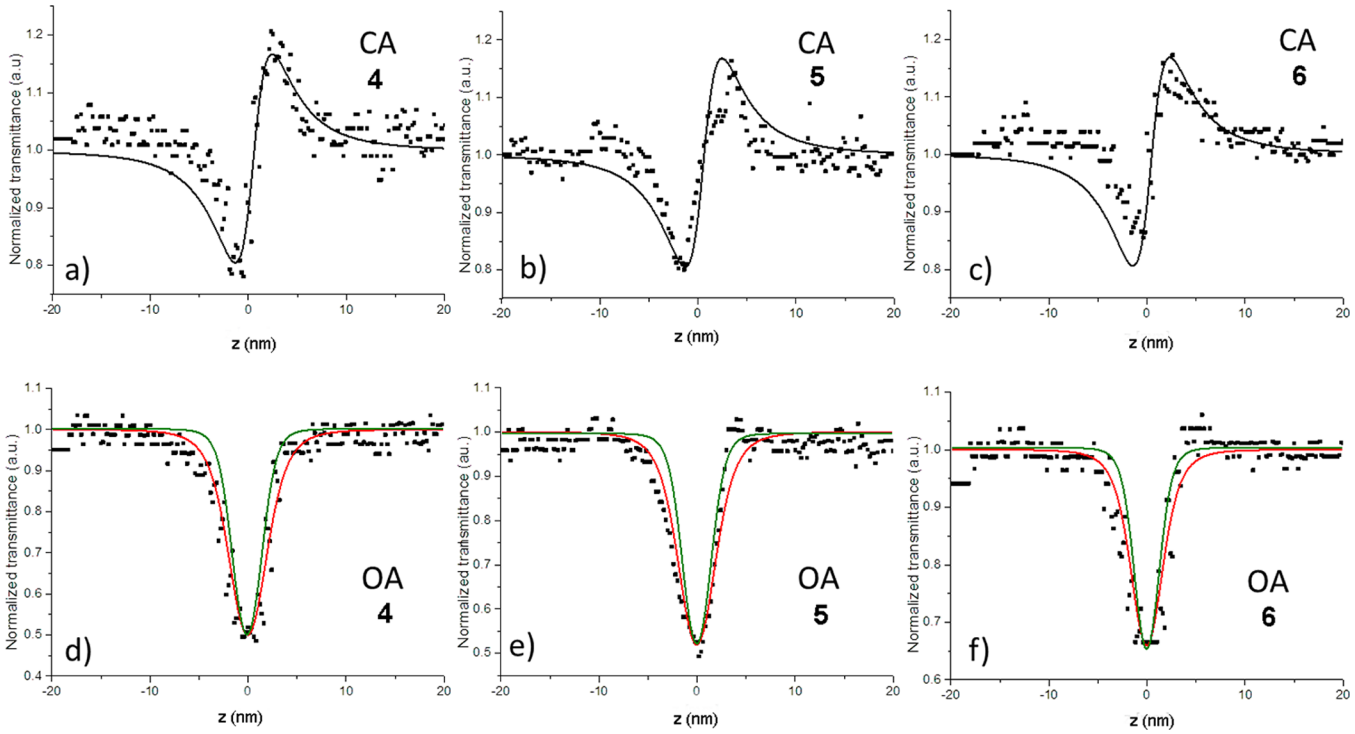

Figure 8. Representative Z-scan traces for dyes **4**–**6**: (a–c) closed aperture (CA) and (d–f) open aperture (OA) at 111 GW cm^{-2} with femtosecond pulses at 960 nm. Theoretical fits are shown for 3PA (solid red curves) and 4PA (solid green curves).

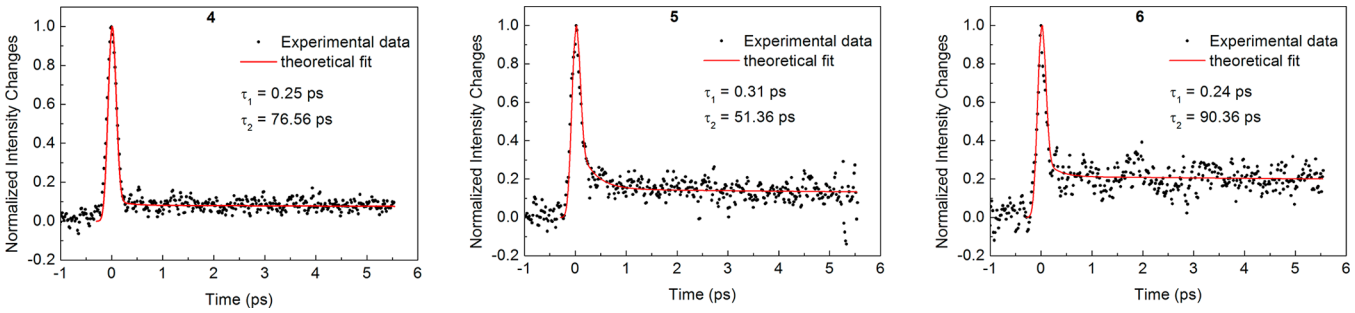

Figure 9. Changes in the probe beam intensity measured for the samples **4**–**6** together with the fitted theoretical decay curves.

CA traces were similar for all wavelengths, the beam exhibiting defocusing before and focusing after the focal plane, which is characteristic for positive (self-focusing) refractive nonlinearity. The differences between CA traces for the solutions of the dyes and those for the cuvettes with the solvent alone can be used to determine the nonlinear refraction properties of the dyes (due to real parts of the third-order polarizability and other odd higher-order polarizabilities), but this has not been followed in the present work, since the nonlinear refraction in strong nonlinear absorption wavelength ranges is of little practical significance. A dip in the OA traces at the focus is seen in all curves, indicating 2PA and/or multiphoton absorption. As judged by the criterion of the fit between the experimental open-aperture scan and theoretical line shapes, different numbers of photons can be assumed to be absorbed simultaneously. The solid red lines in Figure 8d–f represent 3PA and the solid green lines 4PA. At a wavelength of 960 nm 3PA seems to be dominant, although some contribution of 4PA may also be assumed. In addition, in each of the discussed cases (**4**–**6**) the OA dip seems to deviate a bit from being perfectly symmetrical, which may indicate that additional photochemical processes may be taking place during the measurements.

Pump–Probe Experiments. In order to elucidate the mechanism of the multiphoton absorption for the studied dyes, degenerate pump–probe experiments (the beam and probe wavelengths being the same) were also performed. Such measurements provide a way to distinguish between instantaneous multiphoton absorption due to higher-order optical nonlinearities (for example, 3PA is related to the imaginary part of the fifth-order molecular polarizability) and sequential processes, as for example absorption of a third photon by two-photon prepared excited states. In the present case the results point out the presence of sequential processes, as the obtained signal clearly shows two components: a fast component, corresponding roughly to autocorrelation of the laser pulses, and a slow tail due to excited-state absorption. However, since the amplitude of the signal in the tail is much smaller than that in the peak due to the instantaneous processes, it can be concluded that the relative importance of excited-state absorption is lower than that of the direct three-photon absorption. Changes in the probe beam intensity after

DOI: 10.1021/acs.joc.5b01636
J. Org. Chem. 2015, 80, 9641–9651

passing the samples and the theoretical fits are presented in Figure 9. It should be noted that the signals, measured with a lock-in amplifier, correspond to a decrease in the transmittance. The best fits of the theoretical decay curves to the experimental results obtained using the formalism given in ref 38 have been achieved assuming a double-exponential decay. The short time constant is close to the value of the pulse duration; thus, it is not likely to reflect a relaxation process and the longer time constant should be attributed to the relaxation of the states excited by absorption of two photons.

Multiphoton Excited Fluorescence (MPEF). Two-photon absorption cross sections (δ_{2PA}) were also evaluated by the two-photon-induced fluorescence technique using femtosecond laser pulses. Representative multiphoton excited fluorescence (MPEF) spectra of the studied dyes in comparison to the one-photon excited emission are shown in Figure 10, while other

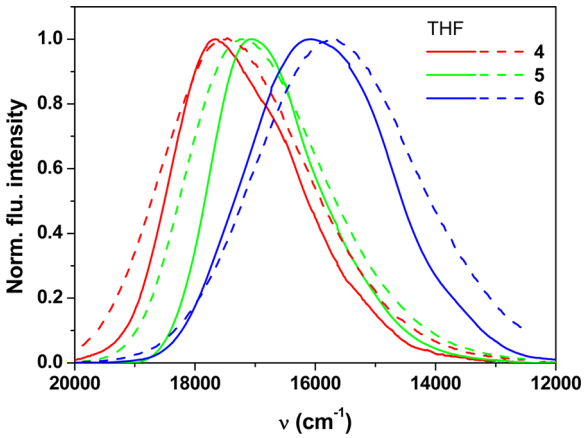

Figure 10. Normalized one-photon (solid line) and two-photon (dotted line) excited fluorescence spectra of 2PA chromophores **4**–**6** in THF.

spectra illustrating changes in the intensity of two-photon-induced fluorescence at different pumped powers at 960 nm are included in Figures S1–S3 in the Supporting Information. As no linear absorption was observed in the range from 600 to 2000 nm, the emission excited by a 960 nm laser wavelength can be attributed to mechanisms involving more than a single-photon absorption.

In comparison with the corresponding one-photon fluorescence, all of the two-photon excited fluorescence spectra of the three compounds have slightly different spectral profiles and peak positions. The maximum peaks of one-photon and two-photon fluorescence are at 572 and 566 nm for chromophore **4**, at 582 and 586 nm for dye **5**, and at 635 and 622 nm for compound **6** in THF. In comparison with the corresponding one-photon fluorescence, a blue shift for two-photon fluorescence is obtained for **4** and **6**, whereas for the dye **5** a bathochromic shift is observed. These differences may be due to different excitation modes of the chromophores.[39,40]

To confirm the nonlinear absorption mechanism, the integrated fluorescence intensities were plotted vs laser beam intensity, as shown in Figure 11. In all cases, the slopes of the log–log dependences of the fluorescence intensity upon irradiation intensity were found to be greater than 2, the value expected for a 2PA mechanism. In fact, they were ca. 3.4–3.7, indicating that the process of the excitation at 960 nm involves more than two photons.

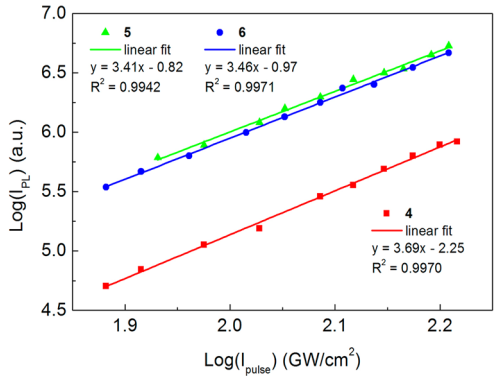

Figure 11. Dependence of the fluorescence intensity upon irradiation intensity under multiphoton excitation.

Nevertheless, we calculated (on the basis of eq 2, vide infra) the effective two-photon absorption (2PA) cross section from the fluorescence measurement using the formalism and reference data from work of Makarov et al.[9] First, the quantum efficiencies of the fluorescence of the samples were obtained by measuring the fluorescence of a series of samples at various concentrations using a regular spectrofluorimeter. Rhodamine B was used as the reference dye for that experiment. Samples for effective 2PA cross-section evaluation were prepared at a concentration of 10^{-5} M in THF. We used the same setup as that for the intensity dependence of MPEF. The results are summarized in Table 2. Since the observed phenomena are

Table 2. Photophysical Data[a] of Chromophores 4–6

	σ_2		σ_2/MW	
compd	from 2PF	from Z-scan	from 2PF	from Z-scan
4	570	490	1.37	1.18
5	1100	1950	1.46	2.56
6	1150	2600	1.17	2.63

[a]Definitions and units: two-photon absorption cross sections ($\sigma 2$; *GM*; $1GM = 10^{-50}$ $cm^4 \cdot s \cdot photon^{-1}$), reduced two-photon absorption cross-section ($\sigma 2$/MW; $GM \cdot g^{-1} \cdot mol$).

clearly a combination of several processes, involving sequential absorption (mostly the two-photon absorption followed by one-photon absorption by excited states) and/or three-photon absorption, the interpretation of the results must be cautious. The cross sections presented in Table 2, whether obtained from Z-scan or from fluorescence measurements, are certainly larger than the true TPA cross sections because of the contributions from higher-order processes. The pump–probe data indicate that some part of the response in Z-scan may be due to excited-state absorption. One needs to stress, however, that excited-state absorption should not contribute to the effective 2PA cross-section measured using the MPEF technique, while the instantaneous three-photon absorption should be seen as an increase in an intensity-dependent effective cross section. Altogether, quantitative comparison of the Z-scan and MPEF data should only be attempted with much care, even if all the data are obtained, as in our experiments, at approximately the same laser intensities (around 100 GW/cm^2). With these reservations, some qualitative discussion of the results follows.

As shown in Table 1, the star-type three-branched oxazol-5(4*H*)-ones display larger effective 2PA cross sections than their dipolar counterpart, with the highest σ_2 values for **6** (2600

DOI: 10.1021/acs.joc.5b01636
J. Org. Chem. 2015, 80, 9641–9651

GM). Thus, one can predict that the nonlinear response in the centrosymmetrical derivatives is highly sensitive to the actual interactions among the individual molecular branches. Such interactions might enhance the charge transfer from the core of the 3-fold symmetry structure to its periphery, which obviously should affect the resulting TPA cross-section.[2] Moreover, according to the Z-scan results, the dye **6** has about 50% larger values of δ_2^{PA} than compound **5**. This suggests that increasing the conjugation length by inserting a benzene ring on each branch of the molecule **5** plays a very important role in improving σ_2. However, the reduced 2PA cross section σ_2/MW, which is defined as σ_2 (in GM) divided by the molecular weight (MW), varies as 1.0:2.2:2.2 (calculations based on the Z-scan results) for dyes **4**–**6**, respectively. This means that the molecular weight enables enhanced 2PA cross-section values. However, in the case of the branched compounds, the elongation of the coupling does not affect their nonlinear optical properties to the same extent as the molecular weight. The obtained results indicate some interactions between branches in the molecule, resulting in charge redistribution and extended delocalization. This can result in increased intramolecular charge transfer (ICT) character of the two-photon excitation.[2,41]

While the values of the two-photon absorption cross-section values determined in experimental part of this work are definitely overestimates because of the contributions of higher-order processes, some comparison with the theoretically calculated TPA properties can also be performed (see Table 3). For the calculations of the two-photon absorption probability the quadratic response function formalism[42,43] within the DFT framework was used, as implemented in the DALTON 2011 program.[44,45] Solvent effects were taken into account with the self-consistent reaction field (SCRF) model. All 2PA calculations were carried out employing the CAM-B3LYP[46] functional and the 6-311++G(d,p) basis set. The choice of this long-range corrected functional was dictated by the previously conducted studies.[47,48] For similar classes of compounds, the CAM-B3LYP functional leads to a smaller value than the hybrid exchange-correlation B3LYP but is in good accordance with measured values.

Table 3. Computational Data[a] for Chromophores 4 and 5

	σ_2^{cal}	
Γ_F	4	5
0.25	500.61	2283.14
0.4	312.88	1347.60

[a]Definitions and units: calculated two-photon absorption cross sections (σ_2^{cal}), GM, with 1 GM = 10^{-50} cm^4 s photon^{-1}; broadening of the final state (Γ_F), eV.

CONCLUSIONS

One push–pull (**4**) and two star-shaped octupolar (**5** and **6**) compounds based on triphenylamine were prepared with a good overall yield via the "Erlenmeyer azlactone synthesis". The solvent polarity has little effect on the UV–vis absorption spectra, while the emission spectra show systematic bathochromic shifts with an increase in solvent polarity. The emission maxima are spread over a wide range of wavelengths (530–742 nm). This effect is accompanied by a larger Stokes shift in polar solvents due to intramolecular charge transfer. Chromophores **4**–**6** show high multiphoton absorption where contributions of several processes may be simultaneously observed. The effective 2PA cross-section (δ_2^{PA}) in the target compound increased with the branching of the triphenylamine core. The maximum effective 2PA cross sections of the star-shaped three-branched triphenylamines are 1950–2600 GM in the near-infrared region (800–1100 nm). In addition, all chromophores show good photostability. The large effective 2PA cross sections combined with high emission quantum yields and large Stokes shifts make these compounds excellent candidates for various nonlinear absorption applications.

EXPERIMENTAL SECTION

Materials and Methods. All solvents were used without further purification. The aldehydes **1** and **2** used to synthesize oxazolone derivatives **4** and **5** were commercially available. The aldehyde **3**, as a reagent for synthesis of compound **6**, was prepared according to the known procedure.[25] Deuterated solvents for NMR spectroscopic analyses were used as received.

Flash column chromatography was performed using silica gel 60 Å (220–440 mesh) with chloroform as eluent. Analytical thin-layer chromatography (TLC) was carried out on silica gel plates with QF-254 indicator and visualized by UV.

HPLC analyses were done by HPLC systems equipped with a UV–vis detector (the detection wavelength was 450 nm), Binary HPLC pump, and a Symmetry C18 column (3.5 μm, 4.6 × 75 mm). Separation was conducted under isocratic conditions with 1.0 mL/min flow rate at room temperature, 20 μL injection volume, and HPLC grade THF as the mobile phase.

Melting points were checked on an automatic apparatus, applying the capillary method, and the data were not calibrated.

The NMR spectra were recorded in perdeuterated dimethyl sulfoxide (DMSO-d_6) or chloroform ($CDCl_3$) using ^{1}H (400 MHz) and ^{13}C (100 MHz) spectrometers. All chemical shifts are quoted in ppm, relative to tetramethylsilane (TMS), using the residual solvent peak as a reference standard (DMSO-d_6, ∼2.49 ppm (^{1}H) and ∼39.5 ppm (^{13}C); $CDCl_3$, ∼7.24 ppm (^{1}H), ∼77.0 ppm (^{13}C)). Coupling constants (J) are reported in hertz.

The IR spectra were recorded in the range 400–4500 cm^{-1} with a spectral resolution of <2 cm^{-1}.

The steady-state electronic absorption and fluorescence spectra were recorded on a spectrophotometer and a spectrofluorimeter, respectively. The slit width was 5 nm for both excitation and emission. The concentration of dye in solvents of different polarity was either 1.0 × 10^{-5} or 1.0 × 10^{-6} M for absorption and emission measurements, respectively. All measurements have been done at room temperature. The relative fluorescence quantum yields of the oxazolones were obtained by comparing the area under the corrected emission spectrum of the tested sample ($A \approx 0.1$ at 480 nm) with that of a solution of Rhodamine B in ethanol. The reference quantum yield is 0.5 according to the literature.[49] The quantum yield of the tested dyes (Φ_{dye}) was calculated using

$$\Phi_{dye} = \Phi_{ref}\frac{I_{dye}A_{ref}}{I_{ref}A_{dye}}\frac{n_{dye}^2}{n_{ref}^2} \quad (1)$$

where: Φ_{ref} is the fluorescence quantum yield of the reference (Rhodamine B) sample, A_{dye} and A_{ref} are the absorbances of the dye and reference samples at the excitation wavelengths (480 nm), I_{dye} and I_{ref} are the integrated emission intensities for the dyes and reference samples, and n_{dye} and n_{ref} are the refractive indices of the solvents used for the dyes and the reference, respectively.

The fluorescence lifetimes were measured using a single-photon counting system. The apparatus utilizes a picosecond diode laser for the excitation generating pulses of about 81.5 ps at 466.6 nm. Its maximum average power is 5 mW. Short laser pulses in combination with a fast microchannel plate photodetector and ultrafast electronics allow analysis of fluorescence decay signals in the range down to single picoseconds. The dyes were studied at concentrations at which they

DOI: 10.1021/acs.joc.5b01636
J. Org. Chem. 2015, 80, 9641–9651

Scheme 1. Synthesis of Tris[1-(1′-formyl-4,4′-biphenyl)]amine (3)

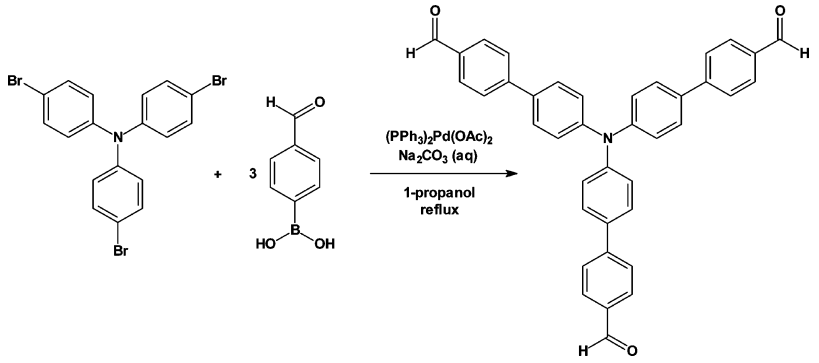

Scheme 2. General Route for the Oxazolone Synthesis

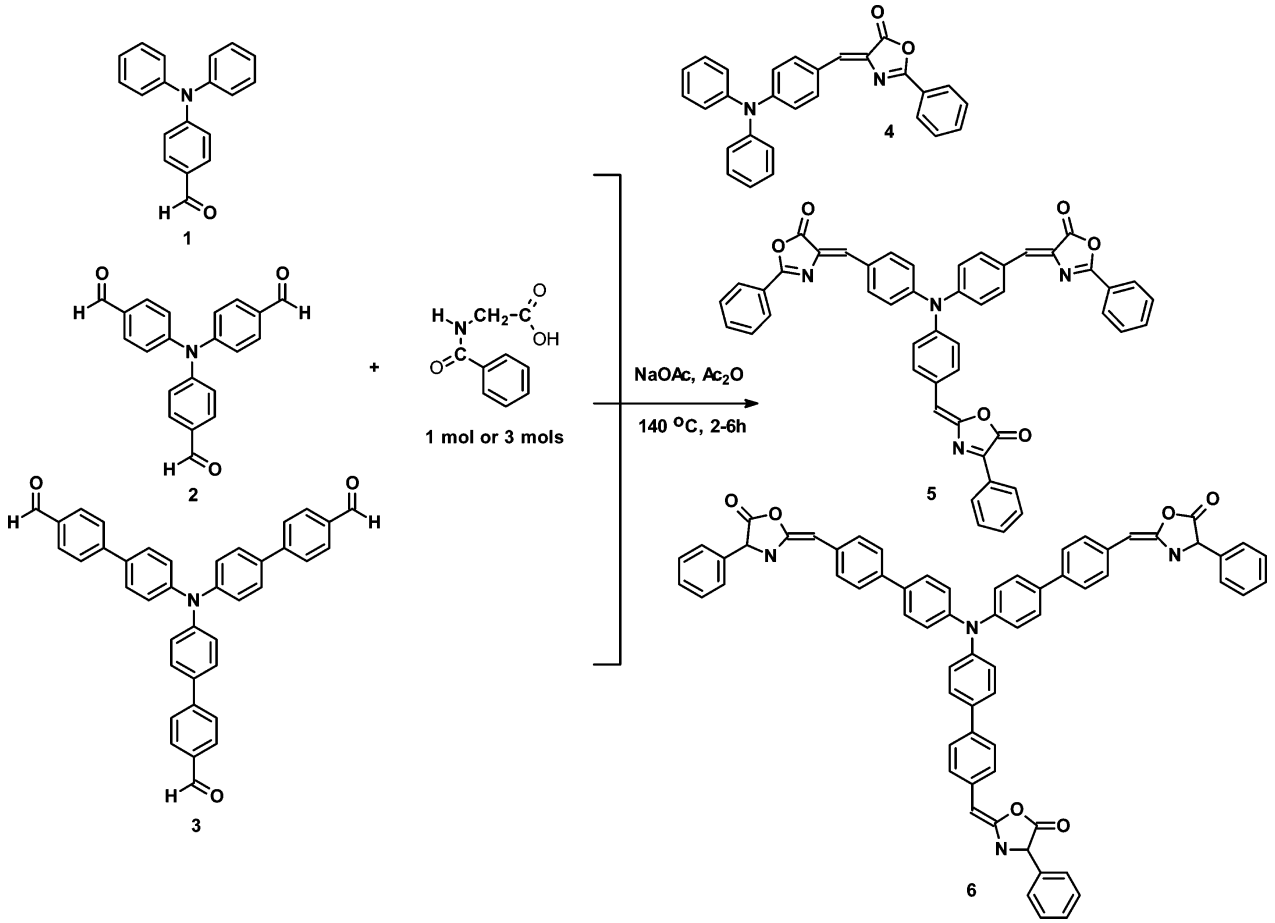

exhibit similar absorbances at 466 nm (ca. 0.1 in a 10 mm cell). The fluorescence decays were fitted to two-exponential functions. The average lifetime, τ_{av}, is calculated as $\tau_{av} = (\sum_i \alpha_i \tau_i)/(\sum_i \alpha_i)$, where α_i and τ_i are the amplitudes and lifetimes.

The photostability of all chromophores was studied in a quartz cuvette with dimensions 4 × 1 × 1 cm. In order to ensure complete absorption of light, the cuvette was placed in a horizontal position and irradiated with 457 nm diode-pumped solid-state (DPSS) laser light at 50 mW through the bottom wall (optical path length 4 cm). The solution was stirred during irradiation.

The 2PA cross sections were determined on the basis of the Z-scan technique[50,51] and the multiphoton excited fluorescence (MPEF) method.[52]

The closed- and open-aperture Z-scan measurements were performed using a setup and procedures described elsewhere.[7,53,54] The laser system consisted of a Quantronix Integra-C regenerative amplifier operating as a 800 nm pump and a Quantronix-Palitra-FS BIBO crystal-based optical parametric amplifier (OPA). The output laser pulses have a pulse duration of ∼130 fs and a repetition rate of 1 kHz. Wavelengths in the range from 600 to 1600 nm were separated from the OPA output using polarizing wavelength separators and color glass filters. The beam was focused by a lens to a focal spot with the beam waist w_0 = 25−60 μm. The calculated intensity at the focus of the setup ranged from 60 to 190 GW/cm^2. The reference, open-aperture (OA), and closed-aperture (CA) signals were detected by three photodiodes, collected by a digital oscilloscope, and transferred to a computer using custom-written software. The Z-scan data obtained on dye solutions were calibrated against closed-aperture measurements on a 4.66 mm thick silica plate.[55,56] The Z-scan measurements were performed in stoppered 1 mm path length cuvettes. Samples were dissolved in THF at concentrations of 10, 5, and 10 mg/5 mL for dyes **4**−**6**, respectively.

DOI: 10.1021/acs.joc.5b01636
J. Org. Chem. 2015, 80, 9641−9651

Spectra of the multiphoton excited fluorescence (MPEF) upon irradiation with 960 nm femtosecond pulses were obtained with an fiber optic spectrograph. Samples in 1 cm fluorescence cuvettes were placed in a four-way cuvette holder with fiber collimating lens, and the spectra were collected at an angle of 90° with respect to the laser beam. An ~4 mm diameter laser beam was focused at the sample with an f = 7.5 cm lens, and the beam power was attenuated by a neutral density filter in the range from 20 to 54 μW, which corresponded to light intensities on the order of 100 GW/cm^2. Higher excitation powers were causing the generation of a white light continuum in THF used as the solvent for the samples. The concentration of dyes **4**–**6** was 10^{-5} M. The effective 2PA cross sections (σ_2) of the dyes were determined by comparing their 2PEF to that of Rhodamine B[9] in methanol (1×10^{-5} M), according to the equation

$$\sigma_2 = \frac{F_s \Phi_r C_r n_s^2}{F_r \Phi_s C_s n_r^2} \sigma_r \quad (2)$$

where the subscripts s and r stand for the sample and reference molecules, respectively. F is the integral area of the two-photon fluorescence, Φ is the fluorescence quantum yield, and C is the number density of the molecules in solution. σ_r is the 2PA cross section of the reference molecule; n stands for the refractive indices of the solvents.

Scheme S1 in the Supporting Information shows the degenerate transient absorption setup used for the pump–probe experiment. In this technique the output beam from the OPA, having a wavelength of 960 nm and pulse width of 140 fs, was split in two to be used as pumping and probing beams. The probing beam was attenuated by neutral density filters and directed through a focusing lens with a focal length of 50 mm straight onto the sample. At the same time, the pump beam was passed through a motorized delay line before being focused on the sample by the same 50 mm lens, so that the two beams overlapped effectively. While the optical path of the pump beam was being made gradually shorter, the delay with which the probe pulse reached the sample with respect to the pomp pulse was elongating. Changes in the probe beam transmittance through the sample were monitored by a photodiode connected to a lock-in amplifier (Signal Recovery). To synchronize the lock-in amplifier, the pump beam was chopped at a frequency set to 165 Hz.

The length of the pulse was measured by putting a BBO crystal in place of the sample at the angle, providing efficient generation of SHG in the autocorrelation beam arising from frequency mixing of probe and pump beams. To determine the decay of the excited states, theoretical curves of convolution of the pump and probe pulses with variable delay were calculated.

Synthetic Procedure. The method of the synthesis of triphenylamine derivatives is based on well-known procedures described in the literature.[25,28,57,58] The synthesis of tris[1-(1′-formyl-4,4′-biphenyl)]-amine (**3**) is outlined in Scheme 1, whereas the general route for oxazolone preparation is shown in Scheme2.

Tris[1-(1′-formyl-4,4′-biphenyl)]amine (3). A 0.029 g portion (0.004 g %) of $(PPh_3)_2Pd(OAc)_2$ was added with vigorous stirring under helium to a degassed suspension of 4.6 g (0.0096 mol) of tris(4-bromophenyl)amine and 5.16 g (0.034 mol) of 4-formylbenzeneboronic acid in 60 mL of 1-propanol. The mixture was stirred at 50 °C for ca. 15 min. Then a solution of potassium carbonate (2 M, 18 mL) and 15 mL of water was added. The resulting mixture was heated to reflux for 5 h under He. The helium was removed after reflux, and another portion of water (60 mL) was added. The reaction mixture was stirred open to the air for 1 h at room temperature. A yellow-green precipitate was filtered off, washed three times with an ethanol/water (1/1, v/v) mixture and three times with ethanol, and dried in vacuo. Yield: 4.7 g (88.7%).

^{1}H NMR (400 MHz, DMSO-d_6): δ (ppm) 7.24–7.26 (d, J = 8.0 Hz, 6H), 7.81–7.83 (d, J = 8.0 Hz, 6H), 7.92–7.94 (d, J = 8.0 Hz, 6H), 7.98–8.00 (d, J = 8.0 Hz, 6H). ^{13}C NMR (100 MHz, DMSO-d_6): δ (ppm) 124.9, 127.3, 128.9, 130.7, 133.9, 135.2, 145.6, 147.4 (CH), 193.1 (CHO). IR (KBr): ν_{max} (cm^{-1}) 3032, 2918, 1700, 1590, 1522, 1491, 1391, 1302, 1283, 1187, 1171, 1060, 817, 714.

(4*Z*)-4-[4-(Diphenylamino)benzylidene]-2-phenyl-1,3-oxazol-5(4*H*)-one (4). A mixture of *N*-benzoylglycine (0.5 g, 2.8 mmol, 1 equiv), *N*,*N*-diphenylbenzaldehyde (0.77 g, 2.8 mmol, 1 equiv), anhydrous sodium acetate (0.23 g, 2.8 mmol, 1 equiv), and acetic anhydride (1.3 mL, 13 mmol, 5 equiv) was refluxed for 4 h. Then, the mixture was cooled to room temperature, diluted with ethanol (5–10 mL), and kept at 0 °C for 20 min. The precipitate was filtered off under suction, washed with cooled ethanol and then with hot distilled water, and dried. The residue was purified by silica gel flash chromatography with chloroform as the eluent to give **4** as a reddish solid. Yield: 57.6% (0.67 g). Mp: 183.2–184.6 °C (lit.[28] mp 168–170 °C). R_f = 0.58.

^{1}H NMR (400 MHz, $CDCl_3$): δ (ppm) 7.06–7.08 (d, $^3J_{H-H}$ = 8.0 Hz, 2H, ArH), 7.18–7.20 (d, $^3J_{H-H}$ = 8.0 Hz, 4H, ArH), 7.21 (t, 2H, ArH), 7.22 (s, 1H, = CHAr), 7.36 (t, 4H, ArH), 7.51 (t, 2H, ArH), 7.58 (t, 1H, ArH), 8.08–8.10 (d, $^3J_{H-H}$ = 8.0 Hz, 2H, ArH), 8.14–8.16 (d, $^3J_{H-H}$ = 8.0 Hz, 2H, ArH). ^{13}C NMR (100 MHz, $CDCl_3$): δ (ppm) 120.3, 124.8, 126.1, 128.0, 128.9, 129.6, 131.9, 132.8, 134.0 (CH), 126.0, 126.3, 129.7, 130.4, 146.3, 150.7, 161.9, 168.1 (C). IR (KBr): ν_{max} (cm^{-1}) 1781, 1767, 1649, 1589, 1548, 1490, 1449, 1371, 1287, 1163, 1027, 985, 888, 819, 763, 698, 505. Anal. Calcd for $C_{28}H_{20}N_2O_2$: C, 80.75; H, 4.84; N, 6.73; O, 7.68. Found: C, 80.74; H, 4.83; N, 6.71.

(4*Z*)-*N*,*N*,*N*-Tris[2-phenyl-4-benzylidene-1,3-oxazol-5(4*H*)-one]amine (5). Chromophore **5** was prepared by the same procedure as described for **4** using *N*-benzoylglycine (1.5 g, 8.4 mmol, 3 equiv), tris(4-formylphenyl)amine (0.92 g, 2.8 mmol, 1 equiv), anhydrous sodium acetate (0.69 g, 8.4 mmol, 3 equiv), and acetic anhydride (3.9 mL, 41 mmol, 15 equiv). Purification was carried out by flash chromatography on silica gel with chloroform as the eluent. Yield: 52.8% (1.12 g). Mp: 287.4–289.3 °C. R_f = 0.33.

^{1}H NMR (400 MHz, $CDCl_3$): δ (ppm) 7.23 (s, 3H), 7.28–7.30 (d, J = 8.0 Hz, 6H), 7.51 (t, 6H), 7.60 (t, 3H), 8.15–8.17 (d, J = 8.0 Hz, 6H), 8.20–8.22 (d, J = 8.0 Hz, 6H). ^{13}C NMR (100 MHz, $CDCl_3$): δ (ppm) 124.6, 128.3, 129.0, 130.6, 133.3, 134.0 (CH), 125.6, 129.7, 132.4, 148.4, 163.1, 167.7 (C). IR (KBr): ν_{max} (cm^{-1}) 1792, 1769, 1651, 1592, 1581, 1504, 1450, 1366, 1288, 1160, 984, 888, 860, 699, 507. Anal. Calcd for $C_{48}H_{30}N_4O_6$: C, 75.98; H, 3.99; N, 7.38; O, 12.65. Found: C, 75.96; H, 4.10; N, 7.32.

(4*Z*)-*N*,*N*,*N*-Tris[2-phenyl-4-(4-phenylbenzylidene)-1,3-oxazol-5(4*H*)-one]amine (6). Chromophore **6** was prepared by the same procedure as described for **4** using *N*-benzoylglycine (0.54 g, 3 mmol, 3 equiv), tris[1-(1′-formyl-4,4′-biphenyl)]amine (0.56 g, 1 mmol, 1 equiv), anhydrous sodium acetate (0.25 g, 3 mmol, 3 equiv), and acetic anhydride (1.4 mL, 15 mmol, 15 equiv). Purification was carried out by flash chromatography on silica gel with chloroform as the eluent. Yield: 49.6% (0.49 g). Mp: 263.0–264.8 °C. R_f = 0.42.

^{1}H NMR (400 MHz, $CDCl_3$): δ (ppm) 7.33 (s, 3H and d, 6H), 7.58 (t, 6H), 7.65 (t, 6H), 7.76–7.78 (d, J = 8.0 Hz, 6H), 8.23–8.25 (d, J = 8.0 Hz, 6H), 8.31–8.33 (d, J = 8.0 Hz, 6H). ^{13}C NMR (100 MHz, $CDCl_3$): δ (ppm) 124.7, 126.9, 128.1, 128.4, 129.0, 131.4, 133.1, 133.4 (CH), 125.7, 132.3, 133.0, 134.7, 142.9, 147.3, 163.4, 167.7 (C). IR (KBr): ν_{max} (cm^{-1}) 1794, 1769, 1652, 1594, 1559, 1492, 1450, 1366, 1326, 1295, 1162, 1109, 982, 887, 860, 818, 778, 699, 580. Anal. Calcd for $C_{66}H_{42}N_4O_6$: C, 80.31; H, 4.29; N, 5.67; O, 9.73. Found: C, 80.34; H, 4.26; N, 5.61.

■ ASSOCIATED CONTENT

Supporting Information

The Supporting Information is available free of charge on the ACS Publications website at DOI: 10.1021/acs.joc.5b01636.

^{1}H, ^{13}C, ^{1}H–^{15}N HMBC, ^{1}H–^{1}H COSY and ^{1}H–^{13}C HMBC NMR and IR spectra of aldehyde **3** and dyes **4**–**6** , HPLC chromatograms, computational details including the optimized geometries (Cartesian coordinates) of the molecules, and 2PEF spectra (PDF)

DOI: 10.1021/acs.joc.5b01636
J. Org. Chem. 2015, 80, 9641–9651

AUTHOR INFORMATION

Corresponding Author

*B.J.: e-mail, beata@utp.edu.pl; fax, +48 52 374 9009; tel, +48 52 374 9034.

Notes

The authors declare no competing financial interest.

ACKNOWLEDGMENTS

This work was supported in part by The Ministry of Science and Higher Education (MNiSW) (Grant No. 9/2014), PL-Grid Infrastructure, and the National Science Centre (DEC-2013/10/A/ST4/00114).

REFERENCES

(1) Lee, K.-S.; Yang, D.-Y.; Park, S. H.; Kim, R. H. *Polym. Adv. Technol.* **2006**, *17*, 72−82.
(2) Han, D.-M.; Feng, J.-K.; Zhao, X.-J.; Ren, A.-M.; Shang, X.-H. *Chem. Phys. Lett.* **2008**, *453*, 129−135.
(3) Boyd, R. *Nonlinear Optics*; Academic Press: New York, 1992.
(4) Fakis, M.; Fitilis, I.; Stefanatos, S.; Vellis, P.; Mikroyannidis, J.; Giannetas, V.; Persephonis, P. *Dyes Pigm.* **2009**, *81*, 63−68.
(5) Xu, C.; Webb, W. W. *J. Opt. Soc. Am. B* **1996**, *13*, 481−491.
(6) Taouri, A.; Derbal, H.; Nunzi, J. M.; Mountasser, R.; Sylla, M. *J. Optoelectron. Adv. M.* **2009**, *11* (11), 1696−1703.
(7) Sheik-Bahae, M.; Said, A. A.; Wei, T. H.; Hagan, D. J.; Van Stryland, E. W. *IEEE J. Quantum Electron.* **1990**, *26*, 760−769.
(8) Wang, D.; Zhou, G. Y.; Ren, Y.; Xu, X. G.; Cheng, X. F.; Shao, Z. S.; Jiang, M. H. *Chem. Phys. Lett.* **2002**, *354*, 423−427.
(9) Makarov, N. S.; Drobizhev, M.; Rebane, A. *Opt. Express* **2008**, *16*, 4029−4047.
(10) Braslavsky, S. E.; Heibel, G. E. *Chem. Rev.* **1992**, *92*, 1381−1410.
(11) Phillip, R.; Sathy, P.; M Nampoori, V. P.; Phillip, J.; Vallabhan, C. P. G. *J. Phys. B: At., Mol. Opt. Phys.* **1992**, *25*, 155−161.
(12) Guerra, M.; Taouri, A.; Marcano, O.; Cabrera, H.; Sylla, M. *Appl. Spectrosc.* **2007**, *61* (10), 1128−1133.
(13) Padilha, L. A.; Webster, S.; Hu, H. H.; Przhonska, O. V.; Hagan, D. J.; Van Stryland, E. W.; et al. *Chem. Phys.* **2008**, *352*, 97−105.
(14) Larson, D. R.; Zipfel, W. R.; Williams, R. M.; Clark, S. W.; Bruchez, M. P.; Wise, F. W.; et al. *Science* **2003**, *300*, 1434−1436.
(15) Mattu, J.; Johansson, T.; Leach, G. W. *J. Phys. Chem. C* **2007**, *111*, 6868−6874.
(16) Terenziani, F.; Katan, C.; Badaeva, E.; Tretiak, S.; Blanchard-Desce, M. *Adv. Mater.* **2008**, *20*, 4641−4678.
(17) Jansik, B.; Salek, P.; Jonsson, D.; Vahtras, O.; Ågren, H. *J. Chem. Phys.* **2005**, *122*, 054107.
(18) Berman, O.; Mukamel, S. *Phys. Rev. A: At., Mol., Opt. Phys.* **2003**, *67*, 42503.
(19) Pawlicki, M.; Hazel, A. C.; Robert, G. D.; Harry, L. A. *Angew. Chem., Int. Ed.* **2009**, *48*, 3244−3266.
(20) Beljonne, D.; Wenseleers, W.; Zojer, E.; Shuai, Z.; Vogel, H.; Pond, S. J. K.; Perry, J. W.; Marder, S. R.; Bredas, J.-L. *Adv. Funct. Mater.* **2002**, *12*, 631−641.
(21) Ramakrishna, G.; Goodson, T., III *J. Phys. Chem. A* **2007**, *111* (6), 993−1000.
(22) Zhou, H.; Zheng, Z.; Xu, G.; Yu, Z.; Yang, X.; Cheng, L.; Tian, X.; Kong, L.; Wu, J.; Tian, Y. *Dyes Pigm.* **2012**, *94*, 570−582.
(23) Chung, S.-J.; Kim, K.-S.; Lin, T.-C.; He, G. S.; Swiatkiewicz, J.; Prasad, P. N. *J. Phys. Chem. B* **1999**, *103*, 10741−10745.
(24) (a) Macak, P.; Luo, Y.; Norman, P.; Ågren, H. *J. Chem. Phys.* **2000**, *113*, 7055−7061. (b) Norman, P.; Luo, Y.; Ågren, H. *J. Chem. Phys.* **1999**, *111*, 7758−7765. (c) Wang, C. K.; Macak, P.; Luo, Y.; Ågren, H. *J. Chem. Phys.* **2001**, *114*, 9813−9820. (d) Cronstrand, P.; Luo, Y.; Ågren, H. *J. Chem. Phys.* **2002**, *117*, 11102−11106.
(25) U.S. Patent Application 0080145698.
(26) El-Mekabaty, A. Erlenmeyer Azlactones: Synthesis, Reactions and Biological Activity. *Int. J. Mod. Org. Chem.* **2013**, *2* (1), 40−66.
(27) Chen, K.-Y.; Cheng, Y.-M.; Lai, C.-H.; Hsu, C.-C.; Ho, M.-L.; Lee, G.-H.; Chou, P.-T. *J. Am. Chem. Soc.* **2007**, *129*, 4534−4535.
(28) Rafiq, S.; Rajbongshi, B. K.; Nair, N. N.; Sen, P.; Ramanathan, G. *J. Phys. Chem. A* **2011**, *115*, 13733−13742.
(29) Angulo, G.; Grampp, G.; Rosspeintner, A. *Spectrochim. Acta, Part A* **2006**, *65*, 727−731.
(30) Birks, J. B.; Dyson, D. J. *Proc. R. Soc. London, Ser. A* **1963**, *275*, 135−148.
(31) Suppan, P. *J. Photochem. Photobiol., A* **1990**, *50*, 293−330.
(32) Jędrzejewska, B.; Kabatc, J.; Ośmiałowski, B.; Pączkowski, J. *Spectrochim. Acta, Part A* **2007**, *67*, 306−315.
(33) Shao, J.; Guan, Z.; Yan, Y.; Jiao, C.; Xu, Q.-H.; Chi, C. *J. Org. Chem.* **2011**, *76*, 780−790.
(34) Hrobáriková, V.; Hrobárik, P.; Gajdoš, P.; Fitilis, I.; Fakis, M.; Persephonis, P.; Zahradnĭk, P. *J. Org. Chem.* **2010**, *75*, 3053−3068.
(35) Yan, Y. L.; Li, B.; Liu, K. J.; Dong, Z. W.; Wang, X. M.; Qian, S. X. *J. Phys. Chem. A* **2007**, *111*, 4188−4194.
(36) Samoć, M.; Morrall, J. P.; Dalton, G. T.; Cifuentes, M. P.; Humphrey, M. G. *Angew. Chem., Int. Ed.* **2007**, *46*, 731−733.
(37) Hańczyc, P.; Samoć, M.; Norden, B. *Nat. Photonics* **2013**, *7* (12), 969−972.
(38) Pang, Y.; Samoć, M.; Prasad, P. N. *J. Chem. Phys.* **1991**, *94*, 5282−5290.
(39) Cui, J.; Fan, J.; Peng, X.; Sun, S. *Dyes Pigm.* **2011**, *89*, 330−335.
(40) Qian, Y.; Meng, K.; Lu, C.-G.; Lin, B.-P.; Huang, W.; Cui, Y.-P. *Dyes Pigm.* **2009**, *80*, 174−180.
(41) Vivas, M. G.; Silva, D. L.; De Boni, L.; Bretonniere, Y.; Andraud, C.; Laibe-Darbour, F.; Mulatier, J.-C.; Zaleśny, R.; Bartkowiak, W.; Canuto, S.; Mendonca, C. R. *J. Phys. Chem. B* **2012**, *116*, 14677−14688.
(42) Olsen, J.; Jorgensen, P. *J. Chem. Phys.* **1985**, *82*, 3235−3264.
(43) Sałek, P.; Vahtras, O.; Guo, J. D.; Luo, Y.; Helgaker, T.; Ågren, H. *Chem. Phys. Lett.* **2003**, *374*, 446−452.
(44) *DALTON, A molecular electronic structure program*; Release Dalton 2011 (2011); see http://daltonprogram.org/.
(45) *LSDALTON, A linear scaling molecular electronic structure program*; Release Dalton 2011 (2011); see http://daltonprogram.org.
(46) Yanai, T.; Tew, D.; Handy, N. *Chem. Phys. Lett.* **2004**, *393*, 51−57.
(47) Krawczyk, P. *J. Mol. Model.* **2010**, *16*, 659−668.
(48) Krawczyk, P. *J. Mol. Model.* **2015**, *21*, 118−136.
(49) Brouwer, A. M. *Pure Appl. Chem.* **2011**, *83* (12), 2213−2228.
(50) Mysliwiec, J.; Szukalski, A.; Sznitko, L.; Miniewicz, A.; Haupa, K.; Zygadlo, K.; Matczyszyn, K.; Olesiak-Bańska, J.; Samoć, M. *Dyes Pigm.* **2014**, *102*, 63−70.
(51) Olesiak-Bańska, J.; Matczyszyn, K.; Zaleśny, R.; Murugan, N. A.; Kongsted, J.; Ågren, H.; Bartkowiak, W.; Samoć, M. *J. Phys. Chem. B* **2013**, *117*, 12013−12019.
(52) Hrobárik, P.; Hrobáriková, V.; Sigmundová, I.; Zahradník, P.; Fakis, M.; Polyzos, I.; Persephonis, P. *J. Org. Chem.* **2011**, *76*, 8726−8736.
(53) Szeremeta, J.; Nyk, M.; Wawrzynczyk, D.; Samoć, M. *Nanoscale* **2013**, *5*, 2388−2393.
(54) Gordel, M.; Olesiak-Bańska, J.; Kolkowski, R.; Matczyszyn, K.; Buckle, M.; Samoć, M. *J. Mater. Chem. C* **2014**, *2*, 7239−7246.
(55) Jędrzejewska, B.; Krawczyk, P.; Gordel, M.; Samoć, M. *Dyes Pigm.* **2014**, *111*, 162−175.
(56) Jędrzejewska, B.; Krawczyk, P.; Pietrzak, M.; Gordel, M.; Matczyszyn, K.; Samoć, M.; Cysewski, P. *Dyes Pigm.* **2013**, *99*, 673−685.
(57) (a) Rodrigues, C. A. B.; Mariz, I. F. A.; Maçôas, E. M. S.; Afonso, C. A. M.; Martinho, J. M. G. *Dyes Pigm.* **2012**, *95*, 713−722; (b) *Dyes Pigm.* **2013**, *99*, 642−652.
(58) Wu, L.; Burgess, K. *J. Am. Chem. Soc.* **2008**, *130*, 4089−4096.

DOI: 10.1021/acs.joc.5b01636
J. Org. Chem. 2015, 80, 9641−9651